ACS APPLIED MATERIALS & INTERFACES

Research Article

www.acsami.org

$Mg(OH)_2$ Supported Nanoscale Zero Valent Iron Enhancing the Removal of Pb(II) from Aqueous Solution

Minghui Liu,[†,∥] Yonghao Wang,[†,‡,∥] Luntai Chen,[†,∥] Yan Zhang,[†,∥] and Zhang Lin*[,†,§,∥]

[†]Key Laboratory of Design and Assembly of Functional Nanostructures, Fujian Institute of Research on the Structure of Matter, Chinese Academy of Sciences, Fuzhou, Fujian 350002, China

[‡]College of Environment and Resources, Fuzhou University, Fuzhou, Fujian 350002, China

[§]School of Environment and Energy, South China University of Technology, Guangzhou 510006, China

[∥]Fujian Provincial Key Laboratory of Nanomaterials, Fujian Institute of Research on the Structure of Matter, Chinese Academy of Sciences, Fuzhou, Fujian 350002, China

S *Supporting Information*

ABSTRACT: In this article, a novel composite ($Mg(OH)_2$ supported nanoscale zerovalent iron (denoted as nZVI@Mg-$(OH)_2$) was prepared and characterized by X-ray diffraction, scanning electron microscopy, and transmission electron microscopy method. The morphology analysis revealed that $Mg(OH)_2$ appeared as self-supported flower-like spheres, and nano Fe^0 particles were uniformly immobilized on the surface of their "flower petals", thus aggregation of Fe^0 particles was minimized. Then the Pb(II) removal performance was tested by batch experiments. The composite presented exceptional removal capacity (1986.6 mg/g) compared with $Mg(OH)_2$ and nanoscale zerovalent iron due to the synergistic effect. Mechanisms were also explored by a comparative study of the phase, morphology, and surface valence state of composite before and after reaction, indicating that at least three paths are involved in the synergistic removal process: (1) Pb(II) adsorption by $Mg(OH)_2$ (companied with ion exchange reaction); (2) Pb(II) reduction to Pb^0 by nanoscale zerovalent iron; and (3) Pb(II) precipitation as $Pb(OH)_2$. The hydroxies provided by $Mg(OH)_2$ can dramatically promote the role of nanoscale zerovalent iron as reducer, thus greatly enhancing the whole Pb(II) sequestration process. The excellent performance shown in our research potentially provides an alternative technique for Pb(II) pollution treatment.

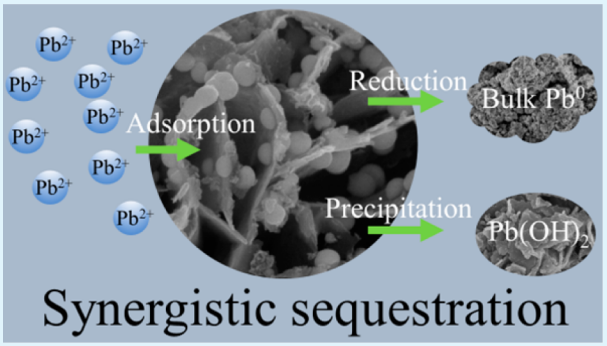

KEYWORDS: *nanoscale zerovalent iron (nZVI), magnesium hydroxide, nZVI@Mg(OH)$_2$ composite, synergistic sequestration*

INTRODUCTION

Lead can cause acute, chronic circulatory, neurological, hematological, gastrointestinal, reproductive, and immunological pathologies,[1−3] because of its toxicity and nonbiodegradability. In China, some industrial processes including lead mining, smelting, and consuming can discharge lead-bearing wastewater, especially in the lead-acid batteries industry, where over 20 million tons of wastewater are generated per year, containing more than 150 tons of Pb(II). Therefore, a cost-effective method must be developed to treat Pb(II)-bearing wastewater.

At present, extensive methods have been employed to remedy heavy metal polluted wastewater, including chemical precipitation, ion-exchange, membrane separation, and adsorption.[4−6] Among them, adsorption is considered as one of the most attractive ways due to its easy processability and high efficiency. In the past two decades, nanoscale zerovalent iron (nZVI) has received much attention because of its large specific surface area, high reaction activity, and strong reductive power.[7,8] Studies show that nZVI appears to be effective in removing various pollutants, such as chlorinated organic compounds,[9] nitroaromatic compounds,[10] dyes,[11] and heavy metal ions,[12−15] including Pb(II).[16−21] Nevertheless, nZVI particles tend to aggregate due to the high surface energy and magnetic force, leading to sharp deterioration of activity, durability, and efficiency, which would greatly hinder the large-scale application of nZVI.[22] Incorporating nZVI particles onto support materials can successfully ease the above-mentioned problems. The commonly used support materials include kaolinite,[11,17] zeolite,[20] clay,[23,24] bentonite[25] and chelating resin,[16] mesoporous carbon,[10,14] silica,[9] and graphene,[26] which all can reduce the aggregation of nZVI particles, thus improving their performance in pollutant treatment. However, some shortcomings of the reported support materials, such as complexity of preparation, high cost, and uneven loading, still limit the wide application of nZVI. Hence, the ideal carrier to

Received: December 30, 2014
Accepted: March 31, 2015
Published: March 31, 2015

ACS Publications © 2015 American Chemical Society

DOI: 10.1021/am509184e
ACS Appl. Mater. Interfaces 2015, 7, 7961−7969

fulfill the potential of nZVI must be cost-effective, mechanically stable, and compatible with nZVI particles. Especially, an intense affinity of support material toward target ions will definitely enhance the performance of nZVI as a whole.

In recent years, nanoscale magnesium hydroxide ($Mg(OH)_2$) has aroused extensive attention because of low-cost and environmental friendliness. Researches indicate that $Mg(OH)_2$ exhibits a promising prospect in acid wastewater treatment, heavy metal deprivation,[27] and decoloration of printing and dyeing wastewater. For instance, Wang et al.[28] demonstrated that nanoscale self-supported $Mg(OH)_2$ aggregates could absorb low concentration anionic dye from water selectively. Li et al.[29] reported that self-supported flowerlike $Mg(OH)_2$ could recycle rare earth ion from low concentration wastewater via ion-exchange. All those researches reveal that the morphology of $Mg(OH)_2$ can be easily controlled and modified to obtain a self-supported flowerlike structure with large specific surface area, which can potentially provide an ideal carrier for nZVI particles.[30] Based on the potential attraction of $Mg(OH)_2$ to Pb(II), we expected the combination of nZVI and $Mg(OH)_2$ could allow a synergy more than reducing aggregation of nZVI particles, which would facilitate decontamination of Pb(II).

In this article, we aim to develop a novel composite by loading nZVI onto $Mg(OH)_2$ (nZVI@$Mg(OH)_2$). The performance of removing Pb(II) was investigated by batch experiments. In addition, the influence of Fe loading ratio, pH value, and initial Pb(II) concentration on removal efficiency were also tested. The results show that the agglomeration of nZVI particles was eliminated, and a superb capacity for Pb(II) uptake was achieved (1986.6 mg/g), much higher than the weighted sum value (1246 mg/g) of its component, indicating the existence of a synergy between nZVI and $Mg(OH)_2$. Further mechanism analyses attested that $Mg(OH)_2$ played a crucial role by releasing OH^- which can enhance the reduction of Pb(II).

EXPERIMENTAL SECTION

Materials and Chemicals. All chemicals used in this study, including magnesium sulfate ($MgSO_4·7H_2O$), sodium borohydride ($NaBH_4$), lead acetate ($Pb[CH_3COO]_2·3H_2O$), ferrous sulfate ($FeSO_4·7H_2O$), sodium hydroxide, acetic acid (CH_3COOH), and nitric acid (HNO_3), were analytic grade purchased from Sinopharm Chemical Reagent Shanghai Co. Ltd. and were used directly as received without further purification. All solutions were prepared using nanopure water (conductivity = 18 $\mu\Omega$/m, Toc < 3 μg/L). A stock solution of Pb(II) was prepared by dissolving 1.8306 g of lead acetate ($Pb[CH_3COO]_2·3H_2O$) into 1000 mL of nanopure water at a volumetric flask, and a Pb(II) solution of different concentrations was made by dilution of the stock solution.

Preparation of $Mg(OH)_2$, nZVI and nZVI@$Mg(OH)_2$ Composite. $Mg(OH)_2$ was prepared through facile precipitation method at room temperature and atmospheric pressure. Briefly, NaOH (1 M) solution was introduced into the same volume of $MgSO_4$ (0.5M) $C_3H_8O_3/H_2O$ hybrid solution (15:85, v/v) dropwise, while stirring vigorously through the titration, and it was continuously stirred for another 6 h after the titration. After aging for 24 h, the precipitate was collected by centrifugation and followed by washing with nanopure water and absolute ethanol several times and then dried at 50 °C for use.

A modified liquid phase sodium borohydride reduction method[31] was employed to prepare $Mg(OH)_2$ supported nZVI. In a typical procedure, 0.416 g of $Mg(OH)_2$ was dispersed in 75 mL of absolute ethanol (ultrasonic dispersion for 5 min), 2.085 g of $FeSO_4·7H_2O$ was dissolved in 75 mL of nanopure water, and then the suspension and Fe(II) solution were mixed in a 500 mL three-necked flask to make a Fe(II) concentration of 0.05 M. Then the same volume of 0.25 M $NaBH_4$ was added into the flask through titration with a rate of 3 mL/min. Before and throughout the procedure, N_2 was introduced to expel the dissolved oxygen and keep an anaerobic environment. The flask was stirred at 300 r/min using a mechanical stirrer, and the stirring was continued for another 30 min after finishing the titration. The resulted black paste was collected and washed with nanopure water and absolute ethanol three times respectively, then dried in a vacuum oven at 45 °C overnight, and stored for use. A composite with different Fe content was synthesized through varying the ratio of $Mg(OH)_2$ and $FeSO_4·7H_2O$ (the Fe mass fraction of composite used in following experiments was 53.9% unless specially specified).

Unsupported nZVI was also prepared via the same procedure for comparative study.

Characterizations and Measurements. X-ray diffraction (XRD), scanning electron microscopy (SEM), transmission electron microscopy (TEM), and BET N_2 adsorption method were employed to characterize the as-prepared $Mg(OH)_2$, nZVI, and nZVI@$Mg(OH)_2$ composite.[32] XRD analysis was conducted on a PANalytical X'Pert PRO diffractometer with Cu KR radiation in the continuous scanning mode at 40 kV, 40 mA from 2θ at 5 to 85° with a step size of 0.017°, and collection time of 20 s per step. SEM and TEM images were obtained on a JSM-6700F scanning electron microscopy equipped with an Oxford-INCA energy dispersive X-ray (EDS) spectroscopy and a JEOL JEM2010 transmission electron microscopy at 200 kV. BET surface area of the materials was measured with an ASAP 2020 specific surface area and porosity analyzer (Micromeritics Instrument Corp. U.S.).

Pb(II), Fe(II/III), and Mg(II) concentration in the liquid samples collected from batch experiment was determined by atomic absorption spectrometer (AAS, TAS-990FG, Purkinje General Analytical Instrument corp. China), while Pb, Fe, and Mg element content of solid samples as well as Fe mass fraction of raw composites was determined by inductively coupled plasma-atomic emission spectrometry (ICP-AES, Jobin Yvon Ulima2).

Pb(II) Removal: Batch Experiments. The optimal experimental conditions were determined beforehand, details of the procedure were described in the Supporting Information. Batch experiments for Pb(II) removal, including performances of different materials and effects of different initial Pb(II) concentration were conducted in a 250 mL three-necked flask equipped with a mechanical stirrer at a speed of 300 r/min. The whole set of experiments were conducted at room temperature and N_2 environment (N_2 was introduced 10 min before the experiment started to expel the dissolved oxygen and throughout the procedure to keep an anaerobic environment).

In order to compare the performance of Pb(II) removal by $Mg(OH)_2$, nZVI, and nZVI@$Mg(OH)_2$, 50 mg of each was added into 100 mL of continuously stirred $Pb(CH_3COO)_2$ stock solution of 1000 mg/L. 3 mL of suspension was extracted at certain time intervals and centrifuged to collect both liquid and solid samples. The liquid sample was used for Pb(II), Fe(II/III), and Mg(II) concentration analysis after being filtered by a syringe filter (0.22 μm) and acidized by HNO_3 (0.01 M). The solid sample was dried for Pb, Fe, and Mg element content analysis. The pH value of suspension was monitored and recorded every 1 min during the experiments.

The effect of the initial Pb(II) concentration was tested by the same procedure except the initial concentration was altered to 250, 500, 750, and 1000 mg/L.

To investigate the feasibility toward actual industrial Pb(II)-bearing wastewater, batch experiments were also conducted in acid Pb−Zn mine tailing leachate which was analogous to industrial drainage in terms of strong acidic and high multi-ion concentration solution environment. The method was the same as the optimization experiment.

RESULTS AND DISCUSSION

Characterization of the Materials. Figure 1 demonstrates XRD patterns of nZVI, $Mg(OH)_2$, and nZVI@$Mg(OH)_2$. As shown in Figure 1, the peaks of nZVI are well indexed as ferrite (JCPDS: 00-006-0696), of which 2θ at 44.67, 65.02, and 82.33°

DOI: 10.1021/am509184e
ACS Appl. Mater. Interfaces 2015, 7, 7961−7969

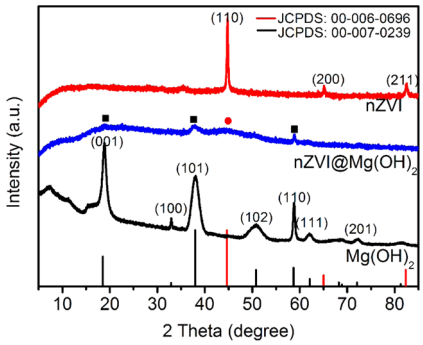

Figure 1. XRD patterns of nZVI, nZVI@$Mg(OH)_2$, and $Mg(OH)_2$ (●, Fe; ■, $Mg(OH)_2$) .

corresponds to [110], [200], and [211] directions of α-Fe, respectively, indicating that unsupported nZVI has high purity and good crystallographic degree.[32,33] The mean grain size of nZVI is calculated to be 22.6 ± 1.1 nm using the Scherrer equation. The XRD pattern of as-prepared Mg(OH)2 is well indexed as brucite (JCPDS: 00-007-0239), with a calculated crystallite size of 21.6 ± 1.1, 31.1 ± 1.5, and 53.9 ± 2.7 nm in the [001], [101], and [110] directions, respectively.[29] However, for nZVI@$Mg(OH)_2$, only weak peaks at 18.53, 37.98, and 58.67° can be recognized, which are coincident with [001], [101], and [110] diffraction peaks of $Mg(OH)_2$. Besides, a peak at 44.67° seems to be formed by broadening the [110] peak of iron, probably due to the low crystallinity degree of iron, which is similar to the previous literature.[31] In addition, the specific surface area is 11.6, 41.3, and 40.2 m^2/g for nZVI, $Mg(OH)_2$, and nZVI@$Mg(OH)_2$, respectively. The high specific surface area is almost maintained after 53.9% Fe loading (determined by ICP-AES), suggesting a well dispersion of nZVI particles.

Figure 2 shows the typical morphology of $Mg(OH)_2$, nZVI, and nZVI@$Mg(OH)_2$. As shown in Figure 2a, as-prepared $Mg(OH)_2$ presents flower-like spheres with uniform size around 10 μm. Enlarged micrograph (Figure S1) reveals that the spheres are formed by interwoven $Mg(OH)_2$ plates with a

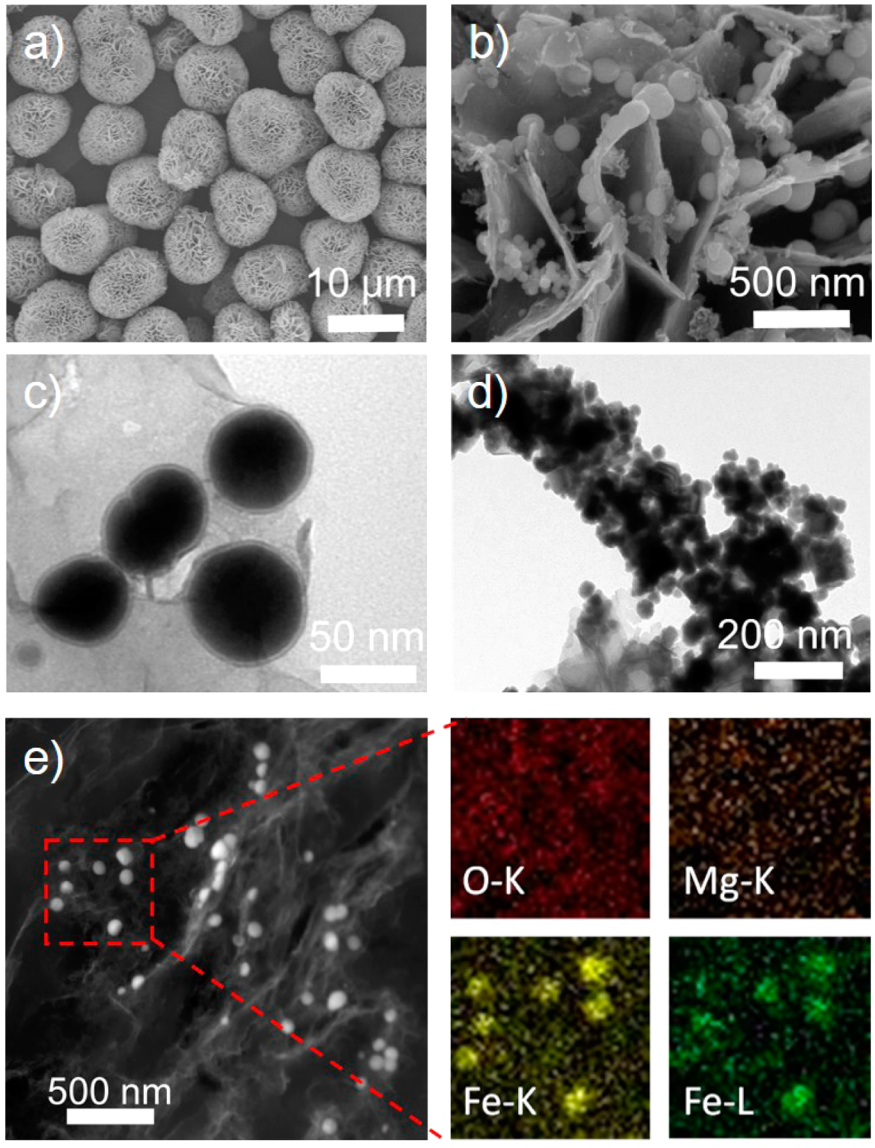

Figure 2. (a) SEM image of flower-like $Mg(OH)_2$ spheres; (b) SEM image of nZVI@$Mg(OH)_2$; (c) TEM image of nZVI@$Mg(OH)_2$; (d) TEM image of nZVI; (e) HAADF-STEM image of nZVI@$Mg(OH)_2$; and corresponding EDS elemental mapping images.

DOI: 10.1021/am509184e
ACS Appl. Mater. Interfaces 2015, 7, 7961−7969

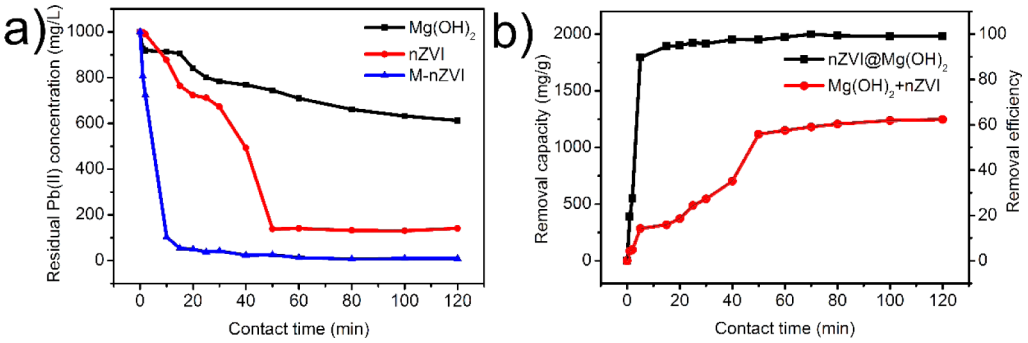

Figure 3. (a) Comparison of Pb(II) removal by nZVI@$Mg(OH)_2$, nZVI, and $Mg(OH)_2$ (dose: 500 mg/L, stirring speed: 300 r/min, initial concentration: 1000 mg/L, initial pH: 6.86, temperature: 25 °C); (b) comparison of Pb(II) removal capacity and efficiency by nZVI@$Mg(OH)_2$ and weighted sum of the value by nZVI and $Mg(OH)_2$ alone.

thickness of 10−20 nm. Morphology of nZVI@$Mg(OH)_2$ in Figure 2b,c reveals that nZVI particles are uniformly immobilized on the surface of $Mg(OH)_2$ plates, and nZVI particles loaded on $Mg(OH)_2$ have a diameter of 40−60 nm and a shell thickness of several nanometers.[19,34] However, similar to previous reports, we can see in Figure 2d that unsupported nZVI particles tend to aggregate together, due to van der Waals' force and magnetic properties of the particles.[18,35] Enlarged TEM images (Figure S3) reveal that the nZVI particles have a diameter of approximately 25 nm, which is consistent with the calculated value through XRD analysis. Moreover, a HAADF-STEM image of nZVI@Mg-$(OH)_2$ and its corresponding EDS elemental mapping images are also presented in Figure 2e. Based on the O−K and Mg−K signals and their distribution area, we find that the lamellar structure in designated area is $Mg(OH)_2$ and Fe−K and Fe-L signal confirmed the particles belong to Fe (or its oxide), which certified the component of nZVI@$Mg(OH)_2$ together with morphologic analysis.[33]

Pb(II) Removal from Water. The optimization experiments suggest that Pb(II) removal can be processed with a neutral pH and 50% Fe content in composite (Figure S5).[19] The study also shows that the initial Pb(II) concentration can barely influence the removal performance. Despite the fact that the initial concentration varies from 250 to 1000 mg/L, more than 90% of Pb(II) is removed within 20 min for all samples. Especially, when the initial concentration is lower than 750 mg/L, no Pb(II) is detected after 120 min (Figure S6).

Figure 3 presents the performance of Pb(II) removal by $Mg(OH)_2$, nZVI, and nZVI@$Mg(OH)_2$ under the same optimal condition. As shown in Figure 3a, the Pb(II) concentration decreases from the initial 1000 mg/L to 623.2, 141.8, and 6.8 mg/L after 120 min. The removal capacity of Pb(II) for each material is calculated to be 775.4, 1718.4, and 1986.6 mg/g. The curves in Figure 3a show that the Pb(II) concentration decreases slowly for $Mg(OH)_2$, while it occurs a quick decline with fluctuant rate for unsupported nZVI. As for nZVI@$Mg(OH)_2$, the Pb(II) concentration drops more quickly and ends with much lower residual concentration.[16,18] Compared to $Mg(OH)_2$ and nZVI, the removal performance of the composite has obviously improved. To verify that the improvement resulted from the synergistic effect of $Mg(OH)_2$ and nZVI, a weighted sum of capacity (as defined in formula 1) was calculated.

$$Q_{weightedsum} = Q_{nZVI}wt\%_{nZVI} + Q_{Mg(OH)_2}wt\%_{Mg(OH)_2} \quad (1)$$

where Q_{nZVI} and $Q_{Mg(OH)_2}$ are the uptake amounts of Pb(II) by nZVI and $Mg(OH)_2$ under the same experimental conditions. wt $\%_{nZVI}$, wt $\%_{Mg(OH)_2}$ are weight percentages of nZVI and $Mg(OH)_2$ in the nZVI@$Mg(OH)_2$ composite. As shown in Figure 3b, the values of capacity and efficiency are 1246 mg/g and 62%, far less than that of nZVI@$Mg(OH)_2$. Table 1 lists

Table 1. Comparison of Pb(II) Removal Performance of nZVI@$Mg(OH)_2$ with Other nZVI Based Materials Reported Previously[a]

	specific surface area (m^2/g)			capacity (mg/g)		
materials	nZVI	S.M.	comp.	nZVI	S.M.	comp.
nZVI@$Mg(OH)_2$ composite (this study)	11.6	41.3	40.2	1718.4	775.4	1986.6
nZVI-Zeolite composite[20]	12.3	1.0	83.4			806.0
nZVI-Graphene composite[26]				455.9		585.5
Sineguelas waste supported nZVI[36]		3.9	35.6		63.5	225.0
Kaolin supported nZVI[17]		3.7	26.1			440.5

[a]S.M. = support material, comp. = composite.

the performance of some reported nZVI-based composite for Pb(II) decontamination. Regardless of the varied experiment conditions in each study, to date, the nZVI@$Mg(OH)_2$ composite in this work possesses the highest removal capacity. In addition, we find that unsupported nZVI also exhibits a great capacity (1718.4 mg/g) but still lower than that of nZVI@$Mg(OH)_2$ composite. Therefore, we believe that the synergistic effect and good dispersion of nZVI particles on $Mg(OH)_2$ can improve the removal performance effectively.[18,20,26]

Mechanisms of Pb(II) Removal by nZVI@$Mg(OH)_2$. To better understand the Pb(II) sequestration by the nZVI@$Mg(OH)_2$ composite, the variations in phase, morphology, surface valence state of composite, and related metal ion concentrations were analyzed utilizing SEM/TEM, XRD, ICP-AES, and high resolution X-ray photoelectron spectrometer (HR-XPS).

Figure 4a illustrates the XRD pattern of the final solid sample after treating 1000 mg/L Pb(II) solution. As shown in Figure 4a, the main phases are indexed as lead (Pb) and lead oxide (PbO), and there is no conspicuous peak attributed to nZVI and $Mg(OH)_2$. Quantitative analyses by Rietveld spectrum

DOI: 10.1021/am509184e
ACS Appl. Mater. Interfaces 2015, 7, 7961−7969

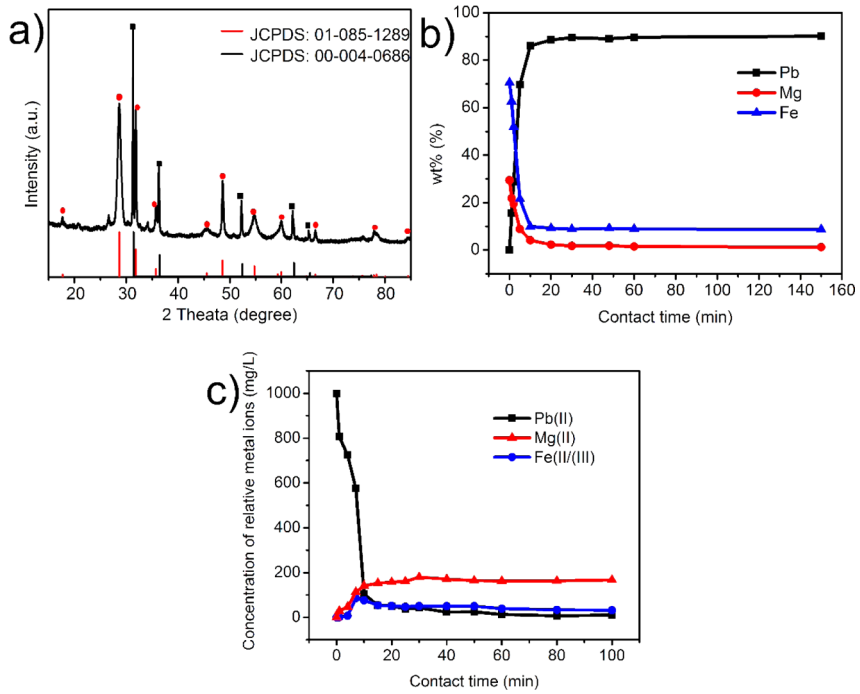

Figure 4. (a) XRD pattern of collected solid material after contacting with Pb(II) solution (dose, 500 mg/L; stirring speed, 300 r/min; contact time, 120 min; initial concentration, 1000 mg/L; initial pH, 6.86; temperature, 25 °C; ■, Pb; ●, PbO); (b) trends of mass fractions (normalized) of relative elements in solid phase; (c)trends of concentrations of relative metal ions in liquid phase during the experiment.

fitting reveal a hybrid phase of 47% Pb and 53% PbO, suggesting that about half of Pb(II) is removed by reduction under the given circumstance. To retell the details of the sequestration process, variation of Pb, Fe, and Mg element distribution in both solid phase and liquid phase are measured during batch experiments. As shown in Figure 4b, Pb mass fraction increases to over 90%, while Fe and Mg drop to 8.66% and 1.2% for the final solid sample. Combined with XRD analysis, the finally obtained solids are mainly comprised of metallic lead and lead oxide. On the contrary, Figure 4c shows that Pb(II) concentration in liquid samples decreases rapidly, while Fe(II/III) and Mg(II) concentrations rise to a certain level, due to the dissolution equilibrium of composite.

Figure 5 exhibits the morphology of nZVI@$Mg(OH)_2$ before and after reacting with Pb(II) solution. As shown in Figure 5c,d, the nZVI@$Mg(OH)_2$ composite still presents a spherical shape and intersection structure after reacting with low concentration (250 mg/L) Pb(II) solution, and the lamellar metallic lead or its compound is formed on the surface. However, when the Pb(II) concentration is increased to 750 mg/L, the intersection structure is destroyed and replaced by lead and its compound packing together closely, in spite of the remaining spherical shape of nZVI@$Mg(OH)_2$ composite. The TEM micrograph (Figure 5b) also gives a clear version of the status of nZVI particles after being treated with low concentration (250 mg/L) Pb(II) solution, among which some are intact and covered with thick-bedded target pollutant, while others are corroded to be smaller-sized fragmentized ones.

HR-XPS was employed to investigate the surface state of Fe, O, and Pb. Figure 6 presents a detailed XPS survey of Fe 2p, O 1s, and Pb 4f regions. In Figure 6a, photoelectron peaks of the Fe 2p region at 711 and 725 eV are attributed to the binding energies of $2p_{3/2}$ and $2p_{1/2}$ of oxidized iron [Fe(III)], and the weak peak at 706.7 eV suggests the existence of zerovalent iron (Fe $2p_{3/2}$), which would disappear after exposure to Pb(II) solution due to extensive oxidization.[34,37] As shown in Figure 6b, the photoelectron spectrum for the O 1s region can be decomposed into three peaks at 529.9, 531.2, and 532.5 eV, which represent the binding energies of different oxygen in O^-, OH^-, and chemically or physically adsorbed water, respectively.[33,37] According to the fitting data recorded by XPS PEAK software (Figure S8), the ratio of O^-, OH^-, and H_2O varied from 63.70%, 29.55%, and 6.75% to 49.54%, 42.68%, and 7.78%, respectively, after reaction. The decrease of the O^- ratio and the increase of the OH^- ratio suggest that the hydroxide, including lead hydroxide and ferric hydroxide, is generated. In Figure 6c, photoelectron peaks at 136.7 and 138.2 eV correspond to Pb^0 and PbO.[19,37] We can see from the figure that the PbO phase is dominant in the final solid samples, while Pb^0 only accounts for 7.16%, which is different from that of the XRD analyses. We believe that the limited penetration depth of the XPS method and the susceptibility to oxidization of metallic lead are responsible for those differences.[16,18]

As the pH value can be a reliable tracer of the reactions during Pb(II) removal, the variation of the pH value was recorded throughout the experiment. As shown in Figure 7a (and Figure S7), without exception, a decline of pH emerges in all nZVI involved processes but is absent when dosed with $Mg(OH)_2$ alone. This phenomenon can be explained by the hydroxylation of Fe(II/III), which can be derived from the following paths: (a) dissolution of iron oxides/hydroxides on the nZVI shell, (b) reaction between zerovalent iron and water,[38] and (c) reduction of Pb(II) by zerovalent iron.[16,33] Since the experiments were conducted under N_2 environment, we presume that the anaerobic environment was well controlled, and the major reactions are listed as eqs 2−6.

$$Mg(OH)_2(s) \rightarrow Mg^{2+} + 2OH^- \quad (2)$$

DOI: 10.1021/am509184e
ACS Appl. Mater. Interfaces 2015, 7, 7961−7969

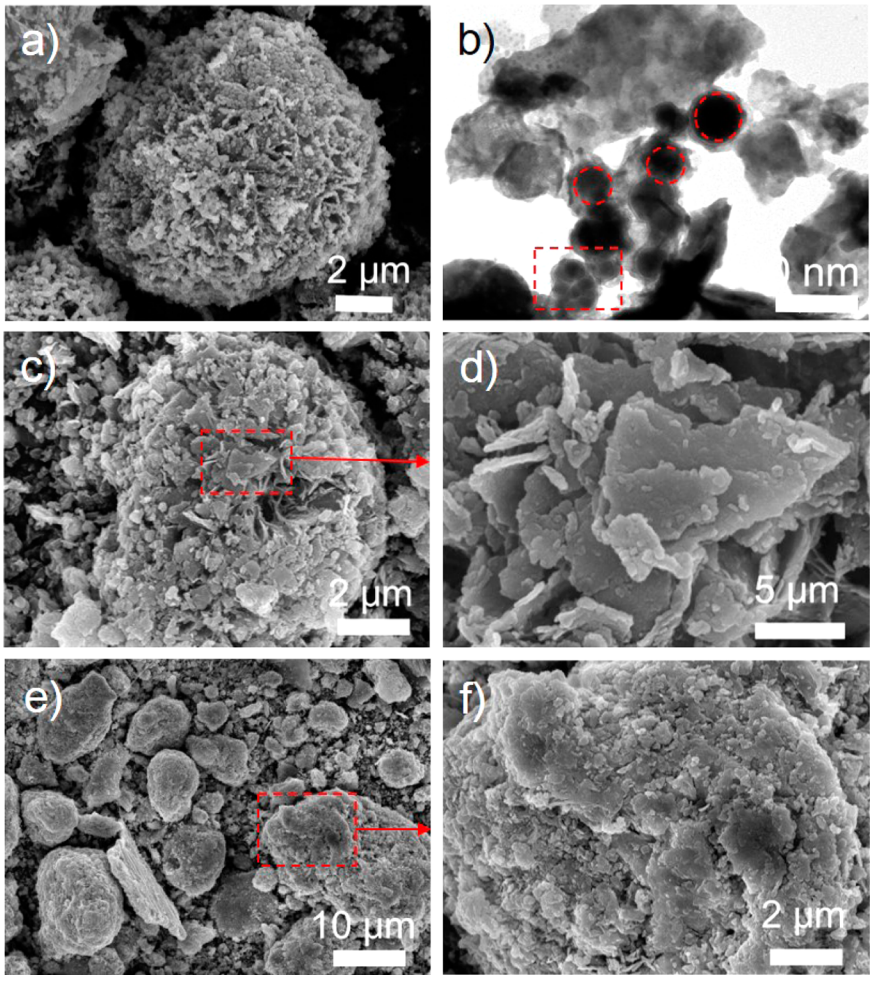

Figure 5. (a) SEM image of nZVI@$Mg(OH)_2$; (b) TEM image; (c and d) SEM images of collected solid material after contacting with low concentration of Pb(II) solution (250 mg/L); (e and f) SEM images of collected solid material after contacting with high concentration of Pb(II) solution (750 mg/L).

$$Pb^{2+} + 2OH^- \rightarrow Pb(OH)_2(s) \quad (3)$$

$$Pb^{2+} + Fe^0(s) \rightarrow Fe^{2+} + Pb^0(s) \quad (4)$$

$$Fe^{2+} + 2H_2O \rightarrow Fe(OH)_2(s) + 2H^+ \quad (5)$$

$$Fe^0(s) + 2H_2O \rightarrow Fe^{2+} + H_2(g) + 2OH^- \quad (6)$$

Based on the analysis above, a mechanism of Pb(II) removal by nZVI@$Mg(OH)_2$ was proposed. In general, Pb(II) was sequestrated through a synergistic process, including adsorption, reduction, ion exchange reaction, and subsequent precipitation.[16,18,19,33,37] According to the variation of the solution pH value, the removal of Pb(II) experienced three stages as shown in Figure 7b.

First, Pb(II) was attracted to the surface of nZVI particles and $Mg(OH)_2$, and then ion exchange reaction was initiated due to the dissolution of $Mg(OH)_2$ (eq 2). At the same time, Pb(II) was partly reduced to Pb^0 by nZVI particles (eq 4), and the hydroxylation of Fe(II) (eq 5) would be triggered when it was accumulated to a certain concentration. The competition of above reactions resulted a slight ascendant of pH value.

Second, the reduction of Pb(II) became dominant, and thus the pH saw a rapid decline caused by the hydroxylation of Fe(II). pH changes of different initial Pb(II) concentrations reveal that a higher initial Pb(II) concentration led to an earlier, larger extent of pH drop (Figure S7), indicating that the pH decline is indeed a consequence of Pb(II) reduction.

Third, The dissolution of $Mg(OH)_2$ continued (eq 2), and the reaction between iron and water (eq 6) proceeded slowly and induced a jump of pH value. Therefore, Pb(II) could be precipitated during this stage (eq 3).

The mechanism analyses suggest that $Mg(OH)_2$ plays an essential role in Pb(II) immobilization for its dispersive, supportive, and nZVI particle aggregate-preventive function as well as its intense inherent affinity to Pb(II). More significantly, a mutual stimulation between reactions 2 and 4 can occur; thus, the hydroxies provided by $Mg(OH)_2$ can dramatically promote the role of nZVI as a reducer. In return, nZVI accelerates the dissolution of $Mg(OH)_2$. The multifunction of $Mg(OH)_2$ makes it a good assistant for nZVI.

Remove Pb(II) from Acid Pb−Zn Mine Tailing Leachate. The results of Pb(II) removal from acid Pb−Zn mine tailing leachate by the nZVI@$Mg(OH)_2$ composite are listed in Table 2. To meet the discharge standard (1.0 mg/L), we varied the dosage from 1000 to 10 000 mg/L and found that the residual concentration of Pb(II) and Zn(II) dropped to 0.22 and 14.2 mg/L, respectively. When the dosage was 7000 mg/L, it corresponded to a removal efficiency of 99.9% and 90.0%. The results certified that Pb(II) could be sequestrated effectively by this composite even under complicated solution

DOI: 10.1021/am509184e
ACS Appl. Mater. Interfaces 2015, 7, 7961−7969

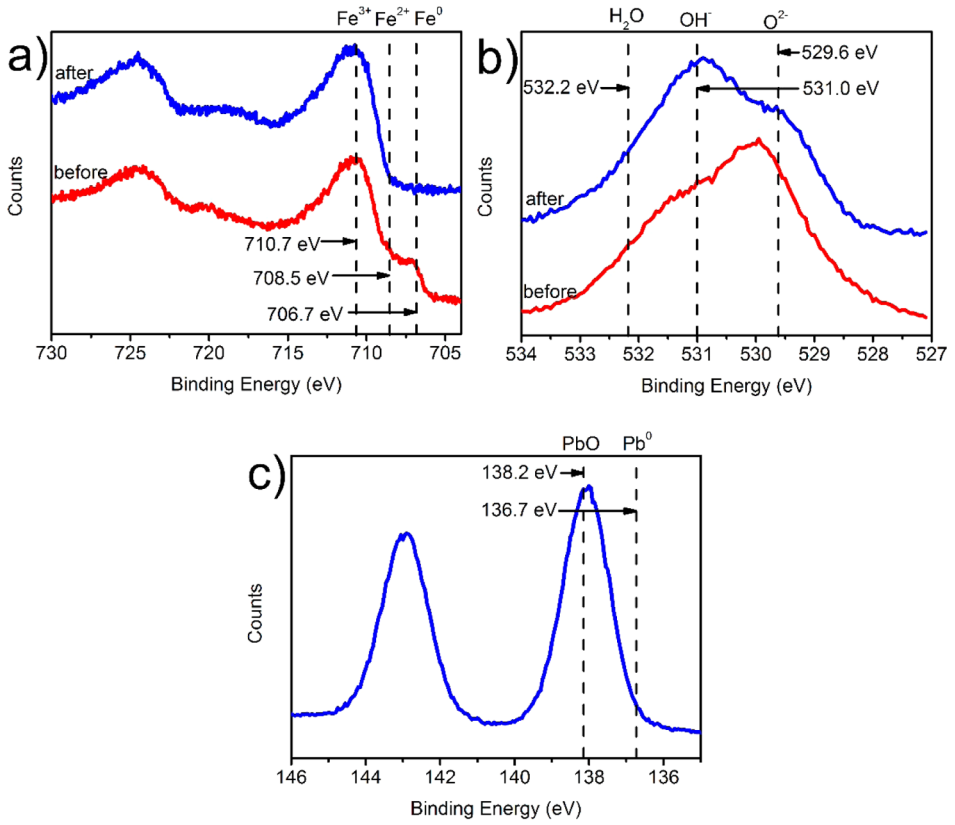

Figure 6. XPS survey of (a) the Fe 2p region, (b) the O 1s region of solid samples before and after treating Pb(II) solution (1000 mg/L), and (c) XPS survey of the Pb 4f region of the final solid sample.

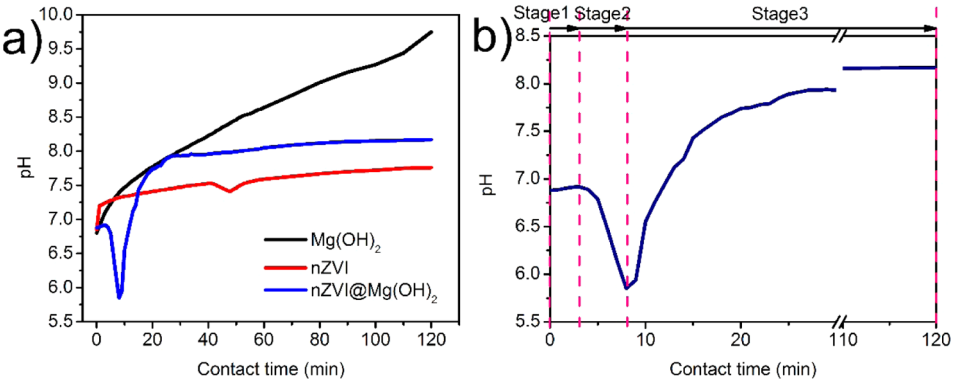

Figure 7. (a) Changes of solution pH during Pb(II) removal by different materials (initial Pb(II) concentration, 1000 mg/L); (b) stages of pH variation during Pb(II) removal by nZVI@$Mg(OH)_2$ (initial Pb(II) concentration, 1000 mg/L).

Table 2. Removal Performance Towards Acid Pb−Zn Mine Tailing Leachate

	Pb(II)	Zn(II)	pH
initial concentration (mg/L)	698.1	201.5	4.8
after neutralized (mg/L)	412.0	142.8	7.0
ultimate concentration (mg/L)	0.22	14.2	7.2
uptake amount (mg/g)	58.4	18.2	-
removal efficiency (%)	99.9	90.0	-

environment. Besides, the outlet pH value was relatively moderate compared to that made by the traditional alkali precipitation method (as high as pH 10).

CONCLUSIONS

In summary, a new Fe^0 containing composite (nZVI@$Mg(OH)_2$) was prepared, characterized, and applied to remove Pb(II). The morphology and phase analyses demonstrated that nZVI particles were successfully loaded on the surface of the self-supported flower-like $Mg(OH)_2$. The results of Pb(II) removal present a superb capacity (1986 mg/g) and large kinetic removal rate (94% uptake within 15 min). We also explored the mechanisms of Pb(II) deprivation, which revealed that $Mg(OH)_2$ can facilitate the sequestration by alleviating aggregation of nZVI particles, enhancing Pb(II) reduction and acting as an absorbent itself. The authors of this article believe that it is the multirole of $Mg(OH)_2$ and the synergistic effect between nZVI and $Mg(OH)_2$ that lead to the exceptional performance of the composite. We think the results of this

DOI: 10.1021/am509184e
ACS Appl. Mater. Interfaces 2015, 7, 7961−7969

work could provide an alternative technique for treating Pb(II)-bearing wastewater.

■ ASSOCIATED CONTENT

Supporting Information

Optimization of operation conditions, Pb(II) removal test in acid Pb−Zn mine tailing leachate, effect of initial concentration, extra SEM and TEM images, and XPS fitting photoelectron spectra. This material is available free of charge via the Internet at http://pubs.acs.org.

■ AUTHOR INFORMATION

Corresponding Author

*Tel.: +86 591 83792630. Fax: +86 591 83705474. E-mail: zlin@fjirsm.ac.cn; zlin@scut.edu.cn.

Notes

The authors declare no competing financial interest.

■ ACKNOWLEDGMENTS

Financial support was provided by the National Basic Research Program of China (2013CB934302 and 2014CB932101), the Outstanding Youth Fund (21125730), the "Strategic Priority Research Program" of the Chinese Academy of Sciences (XDA09030203), the National Science Foundation Grant (21477128), and the Technology Key Project of Fujian Province (2013H0058).

■ REFERENCES

(1) Nemsadze, K.; Sanikidze, T.; Ratiani, L.; Gabunia, L.; Sharashenidze, T. Mechanisms of Lead-Induced Poisoning. *Georgian Med. News* **2009**, *1* (172−173), 92−96.

(2) Hou, S.; Yuan, L.; Jin, P.; Ding, B.; Qin, N.; Li, L.; Liu, X.; Wu, Z.; Zhao, G.; Deng, Y. A Clinical Study of the Effects of Lead Poisoning on the Intelligence and Neurobehavioral Abilities of Children. *Theor. Biol. Med. Modell.* **2013**, *10*, 13.

(3) Yan, C. H.; Xu, J.; Shen, X. M. Childhood Lead Poisoning in China: Challenges and Opportunities. *Environ. Health Perspect.* **2013**, *121* (10), A294−A295.

(4) Zhang, D.; Wang, M.; Tan, Y. L. Preparation of Porous Nano-barium-strontium Titanate by Sorghum Straw Template Method and Its Adsorption Capability for Heavy Metal Ions. *Chin. J. Chem.* **2010**, *68* (16), 1641−1648.

(5) Fu, F.; Wang, Q. Removal of Heavy Metal Ions from Wastewaters: A Review. *J. Environ. Manage.* **2011**, *92* (3), 407−418.

(6) Hua, M.; Zhang, S.; Pan, B.; Zhang, W.; Lv, L.; Zhang, Q. Heavy Metal Removal from Water/Wastewater by Nanosized Metal Oxides: A Review. *J. Hazard. Mater.* **2012**, *211−212*, 317−331.

(7) Crane, R. A.; Scott, T. B. Future Prospects for an Emerging Water Treatment Technology. *J. Hazard. Mater.* **2012**, *211−212*, 112−125.

(8) Yan, W.; Lien, H. L.; Koel, B. E.; Zhang, W. X. Iron Nanoparticles for Environmental Clean-Up: Recent Developments and Future Outlook. *Environ. Sci.: Processes Impacts* **2013**, *15* (1), 63−77.

(9) Zheng, T. H.; Zhan, J. J.; He, J. B.; Day, C.; Lu, Y. F.; Mcpherson, G. L.; Piringer, G.; John, V. T. Reactivity Characteristics of Nanoscale Zerovalent Iron−Silica Composites for Trichloroethylene Remediation. *Environ. Sci. Technol.* **2008**, *42* (12), 4494−4499.

(10) Ling, X.; Li, J.; Zhu, W.; Zhu, Y.; Sun, X.; Shen, J.; Han, W.; Wang, L. Synthesis of Nanoscale Zero-Valent Iron/Ordered Mesoporous Carbon for Adsorption and Synergistic Reduction of Nitrobenzene. *Chemosphere* **2012**, *87* (6), 655−660.

(11) Chen, Z.; Wang, T.; Jin, X.; Chen, Z.; Megharaj, M.; Naidu, R. Multifunctional Kaolinite-Supported Nanoscale Zero-Valent Iron Used for the Adsorption and Degradation of Crystal Violet in Aqueous Solution. *J. Colloid Interface Sci.* **2013**, *398*, 59−66.

(12) Li, X. Q.; Elliott, D. W.; Zhang, W. X. Zero-Valent Iron Nanoparticles for Abatement of Environmental Pollutants: Materials and Engineering Aspects. *Crit. Rev. Solid State Mater. Sci.* **2006**, *31* (4), 111−122.

(13) Fu, F.; Dionysiou, D. D.; Liu, H. The Use of Zero-Valent Iron for Groundwater Remediation and Wastewater Treatment: A Review. *J. Hazard. Mater.* **2014**, *267*, 194−205.

(14) Fu, F.; Han, W.; Huang, C.; Tang, B.; Hu, M. Removal of Cr(VI) from Wastewater by Supported Nanoscale Zero-Valent Iron on Granular Activated Carbon. *Desalin. Water Treat.* **2013**, *51* (13−15), 2680−2686.

(15) Kanel, S. R.; Manning, B.; Charlet, L.; Chol, H. Removal of Arsenic(III) from Groundwater by Nanoscale Zero-Valent Iron. *Environ. Sci. Technol.* **2005**, *39*, 1291−1298.

(16) Ponder, S. M.; Darab, J. G.; Mallouk, T. E. Remediation of Cr(VI) and Pb(II) Aqueous Solutions Using Supported Nanoscale Zero-Valent Iron. *Environ. Sci. Technol.* **2000**, *34* (12), 2564−2569.

(17) Zhang, X.; Lin, S.; Lu, X. Q.; Chen, Z. l. Removal of Pb(II) from Water Using Synthesized Kaolin Supported Nanoscale Zero-Valent Iron. *Chem. Eng. J.* **2010**, *163* (3), 243−248.

(18) Zhang, X.; Lin, S.; Chen, Z.; Megharaj, M.; Naidu, R. Kaolinite-Supported Nanoscale Zero-Valent Iron for Removal of Pb^{2+} from Aqueous Solution: Reactivity, Characterization and Mechanism. *Water Res.* **2011**, *45* (11), 3481−3488.

(19) Zhang, Y.; Su, Y.; Zhou, X.; Dai, C.; Keller, A. A. A New Insight on the Core-Shell Structure of Zerovalent Iron Nanoparticles and Its Application for Pb(II) Sequestration. *J. Hazard. Mater.* **2013**, *263* (Pt 2), 685−693.

(20) Kim, S. A.; Kamala-Kannan, S.; Lee, K. J.; Park, Y. J.; Shea, P. J.; Lee, W. H.; Kim, H. M.; Oh, B. T. Removal of Pb(II) from Aqueous Solution by a Zeolite−Nanoscale Zero-Valent Iron Composite. *Chem. Eng. J.* **2013**, *217*, 54−60.

(21) Mueller, N. C.; Braun, J.; Bruns, J.; Cernik, M.; Rissing, P.; Rickerby, D.; Nowack, B. Application of Nanoscale Zero Valent Iron (NZVI) for Groundwater Remediation in Europe. *Environ. Sci. Pollut. Res. Int.* **2012**, *19* (2), 550−558.

(22) Phenrat, T.; Saleh, N.; Sirk, K.; Tilton, R. D.; Lowry, G. V. Aggregation and Sedimentation of Aqueous Nanoscale Zerovalent Iron Dispersions. *Environ. Sci. Technol.* **2007**, *41* (1), 284−290.

(23) Yu, K.; Gu, C.; Boyd, S. A.; Liu, C.; Sun, C.; Teppen, B. J.; Li, H. Rapid and Extensive Debromination of Decabromodiphenyl Ether by Smectite Clay-Templated Subnanoscale Zero-Valent Iron. *Environ. Sci. Technol.* **2012**, *46* (16), 8969−8975.

(24) Zhang, Y.; Li, Y.; Li, J.; Hu, L.; Zheng, X. Enhanced Removal of Nitrate by a Novel Composite: Nanoscale Zero Valent Iron Supported on Pillared Clay. *Chem. Eng. J.* **2011**, *171* (2), 526−531.

(25) Shi, L. N.; Zhang, X.; Chen, Z. L. Removal of Chromium (VI) from Wastewater Using Bentonite-Supported Nanoscale Zero-Valent Iron. *Water Res.* **2011**, *45* (2), 886−892.

(26) Jabeen, H.; Kemp, K. C.; Chandra, V. Synthesis of Nano Zerovalent Iron Nanoparticles-Graphene Composite for the Treatment of Lead Contaminated Water. *J. Environ. Manage.* **2013**, *130*, 429−435.

(27) Liu, W.; Huang, F.; Wang, Y.; Zou, T.; Zheng, J.; Lin, Z. Recycling $Mg(OH)_2$ Nanoadsorbent During Treating the Low Concentration of Cr^{VI}. *Environ. Sci. Technol.* **2011**, *45* (5), 1955−1961.

(28) Wang, Y. J.; Chen, J.; Lu, L. L.; Lin, Z. Reversible Switch between Bulk $MgCO_3{\cdot}3H_2O$ and $Mg(OH)_2$ Micro/Nanorods Induces Continuous Selective Preconcentration of Anionic Dyes. *ACS Appl. Mater. Interfaces* **2013**, *5* (16), 7698−7703.

(29) Li, C. R.; Zhuang, Z. Y.; Huang, F.; Wu, Z. C.; Hong, Y. P.; Lin, Z. Recycling Rare Earth Elements from Industrial Wastewater with Flowerlike Nano-$Mg(OH)_2$. *ACS Appl. Mater. Interfaces* **2013**, *5* (19), 9719−9725.

(30) Estrada, M.; Costa, V. V.; Beloshapkin, S.; Fuentes, S.; Stoyanov, E.; Gusevskaya, E. V.; Simakov, A. Aerobic Oxidation of Benzyl Alcohol in Methanol Solutions over Au Nanoparticles: $Mg(OH)_2$ Vs MgO as the Support. *Appl. Catal., A* **2014**, *473*, 96−103.

DOI: 10.1021/am509184e
ACS Appl. Mater. Interfaces 2015, 7, 7961−7969

(31) Wang, Q. L.; Sndyder, S.; Kim, J.; Choi, A. Aqueous Ethanol Modified Nanoscale Zerovalent Iron in Bromate Reduction, Synthesis, Characterization, and Reactivity. *Environ. Sci. Technol.* **2009**, *43* (9), 3292−3299.
(32) Sun, Y. P.; Li, X. Q.; Cao, J.; Zhang, W. X.; Wang, H. P. Characterization of Zero-Valent Iron Nanoparticles. *Adv. Colloid Interface Sci.* **2006**, *120* (1−3), 47−56.
(33) Xi, Y.; Mallavarapu, M.; Naidu, R. Reduction and Adsorption of Pb^{2+} in Aqueous Solution by Nano-Zero-Valent Iron—a SEM, TEM and XPS Study. *Mater. Res. Bull.* **2010**, *45* (10), 1361−1367.
(34) Li, X. Q.; Zhang, W. X. Iron Nanoparticles, the Core-Shell Structure and Unique Properties for Ni(II) Sequestration. *Langmuir* **2006**, *22*, 4638−4642.
(35) Li, L.; Fan, M. H.; Brown, R. C.; Leeuwen, J. H. V.; Wang, J.; Wang, W.; Song, Y.; Zhang, P. Synthesis, Properties, and Environmental Applications of Nanoscale Iron-Based Materials: A Review. *Crit. Rev. Env. Sci. Technol.* **2010**, *36* (5), 405−431.
(36) Arshadi, M.; Soleymanzadeh, M.; Salvacion, J. W.; SalimiVahid, F. Nanoscale Zero-Valent Iron (NZVI) Supported on Sineguelas Waste for Pb(II) Removal from Aqueous Solution: Kinetics, Thermodynamic and Mechanism. *J. Colloid Interface Sci.* **2014**, *426*, 241−251.
(37) Li, X. Q.; Zhang, W. X. Sequestration of Metal Cations with Zerovalent Iron Nanoparticles−A Study with High Resolution X-ray Photoelectron Spectroscopy (HR-XPS). *J. Phys. Chem. C* **2007**, *11*, 6939−6946.
(38) Filip, J.; Karlický, F.; Marušák, Z.; Lazar, P.; Černík, M.; Otyepka, M.; Zbořil, R. Anaerobic Reaction of Nanoscale Zerovalent Iron with Water: Mechanism and Kinetics. *J. Phys. Chem. C* **2014**, *118* (25), 13817−13825.

DOI: 10.1021/am509184e
ACS Appl. Mater. Interfaces 2015, 7, 7961−7969